

Nucleosynthesis in a $2M_{\odot}$ He-Flash Pulse Driven Convection Zone

David Stephens

11 December 2017

ABSTRACT

During the asymptotic giant branch (AGB) phase of stellar evolution for a $2M_{\odot}$, $Z = 0.02$ star, the periodic thermal pulses have temperatures as high as 2.9×10^8 K. The $^{22}\text{Ne}(\alpha, n)^{25}\text{Mg}$ can be activated in these conditions leading to a second activation of the s -process after it occurring earlier within the ^{13}C pocket. This adjusts the isotopic per mil ratio of ^{96}Zr and ^{94}Zr , $\delta(^{96}\text{Zr} / ^{94}\text{Zr})$, due to neutron densities reaching $1 \times 10^{10} \text{ cm}^{-3}$ within the He-flash pulse driven convection zone (PDCZ). With modifications to the diffusion coefficient suggested by 3D hydrodynamic stellar convection simulations, the impact of this to the branching of ^{95}Zr is quantified. These changes to the diffusion coefficient adjust the $\delta(^{96}\text{Zr} / ^{94}\text{Zr})$ to better match the observed $\delta(^{96}\text{Zr} / ^{94}\text{Zr})$ measured from pre-solar SiC grains.

Key words: AGB – Convection – Nucleosynthesis – Pre-solar SiC Grains

1 INTRODUCTION

The Zr isotopes are produced from the s -process within stars and ^{56}Fe is the seed. To start the s -process the neutron densities must reach above $1 \times 10^8 \text{ cm}^{-3}$ and in order to affect the Zr isotopes it must pass the first peak at ^{88}Sr . One of the s -process sites in middle mass stars is during the thermal pulses caused by successive He-flashes in their asymptotic giant branch (AGB) phase. In between these thermal pulses the ^{13}C pocket develops and through the $^{13}\text{C}(\alpha, n)^{16}\text{O}$ reaction the s -process occurs. Then, this material will be mixed into the He-flash pulse driven convection zone (PDCZ) and the $^{22}\text{Ne}(\alpha, n)^{25}\text{Mg}$ reaction will activate the s -process again for a few years. The neutron densities that are achieved through these two processes differs significantly and depends on the conditions in the star. The Zr isotopic ratios can be used to understand the conditions within the AGB stars as they are sensitive to the neutron densities that they are exposed to (Battino et al. 2016).

The ^{95}Zr isotope is unstable with a lifetime of 64 days. Within the ^{13}C pocket, the neutron densities do not get large enough to allow for the ^{95}Zr branch to open so most of the ^{95}Zr will decay to ^{95}Mo rather than undergo the neutron capture $^{95}\text{Zr}(n, \gamma)^{96}\text{Zr}$. This skews the isotopic ratios of $^{96}\text{Zr} / ^{94}\text{Zr}$ as there will be production of ^{94}Zr but almost none of ^{96}Zr during the s -process within the ^{13}C pocket. However, once the He-flash PDCZ forms, the $^{22}\text{Ne}(\alpha, n)^{25}\text{Mg}$ reaction can generate neutron densities as large as $1 \times 10^{10} \text{ cm}^{-3}$ which will open the branch for the $^{95}\text{Zr}(n, \gamma)^{96}\text{Zr}$ to occur, shifting the isotopic ratios again. Many of these thermal pulses happen throughout the AGB phase and some of the material left behind from the He-flash PDCZ can be

mixed into the H envelope by the third dredge up that occurs after each thermal pulse. Due to the significant mass loss during the AGB phase, the isotopic ratios of Zr that are well mixed within the outer H envelope can be measured directly from the pre-solar SiC grains that form from this (Barzyk et al. 2006). Battino et al. (2016) compared the H envelope $\delta(^{96}\text{Zr} / ^{94}\text{Zr})$ ratios produced in $3M_{\odot}$ and $2M_{\odot}$ stellar models with the ratios measured in SiC grains from Barzyk et al. (2006). Their results overestimated the ratio in almost all stellar models throughout the AGB phase (Fig. 1).

The goal of this work is to test if minor changes to the diffusion coefficient as a function of mass, as shown by hydrodynamic simulations, will affect the Zr isotopic ratios that the He-flash PDCZ produces. The ratios that are computed with the changes to the diffusion coefficient will be compared to those without and their impact on the results that Battino et al. (2016) predicts will be discussed. The analysis will be conducted on a singular thermal pulse from a $2M_{\odot}$, $Z = 0.02$ stellar model.

2 METHODS AND MODELS

2.1 MESA Models

A $2M_{\odot}$, $Z = 0.02$, stellar evolution model was used and it was computed using the MESA (Paxton et al. 2011) stellar evolution code. A particular model of this type of star was completed by (Ritter et al. 2017). The model used was the $2M_{\odot}$, $Z = 0.02$, star from the NuGrid set1ext, set1.2 model set. These stars were evolved from the pre-main sequence to

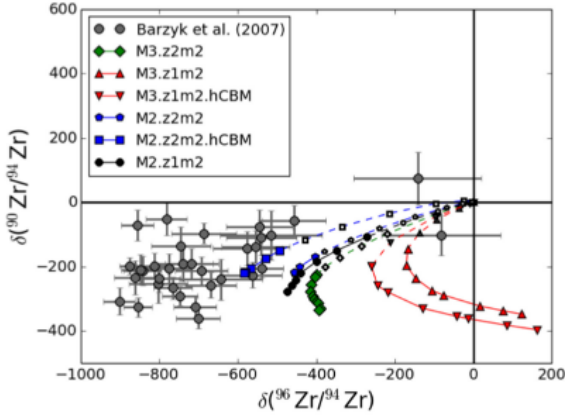


Figure 1. This is a figure from Battino et al. (2016) that contains their stellar model measurements of $\delta(^{96}\text{Zr}/^{94}\text{Zr})$ as well as the SiC grain measurements from Barzyk et al. (2006). The models consistently over predict $\delta(^{96}\text{Zr}/^{94}\text{Zr})$ which is from too much ^{96}Zr being produced in the He-flash PDCZ.

a white dwarf with the nucleosynthesis that does not contribute significantly to energy generation being calculated with `mpnp` for every model. For this work, a single thermal pulse, the 24th, was analyzed and a Kippenhahn diagram of this particular thermal pulse can be seen in Figure 2.

For these models, the mixing lengths theory (Cox & Giuli 1968), MLT, is used to describe the convection zones with a mixing length, $\alpha_{\text{MLT}} = 1.73$. Overshoot is implemented in MESA with the formula from Herwig (2000) and Freytag et al. (1996):

$$D = D_0 \exp^{-2z/fH_{p0}} \quad (1)$$

Where D_0 and H_{p0} are taken at the convective boundary (§2.3) and $f = 0.014$. The methods used in this work to post process the He-flash PDCZ are outlined in §2.5.

2.2 Neutron Density and Temperature

Within the PDCZ, the ^{22}Ne and $^4\text{He}/\alpha$ particles contribute a significant fraction of the mass contained within it. There are a lot of alpha particles from the H-shell burning products from an earlier stage of evolution as well as the helium burning is not significant at this point (Fig. 2). Once temperatures reach close to $T_8 \approx 2.8$ within the PDCZ the $^{22}\text{Ne}(\alpha, n)^{25}\text{Mg}$ reaction is activated. This can be seen from the high neutron densities shown in Figs. 3 and 4. When looking at a particular model number, the neutron density as a function of mass within the convective boundaries has a significant peak near the lower boundary. This is due to the $^{22}\text{Ne}(\alpha, n)^{25}\text{Mg}$ reaction being very sensitive to temperature and a huge portion of the reactions will take place at the bottom of the convection zone. The neutrons will then diffuse/mix throughout the convection zone allowing for the s-process to take place.

In Fig. 3, the average neutron density steadily rises until the point where the convection zone reaches its maximum temperature and then slowly drops. This peak in the average neutron density is very short lived as it is only sustained for a

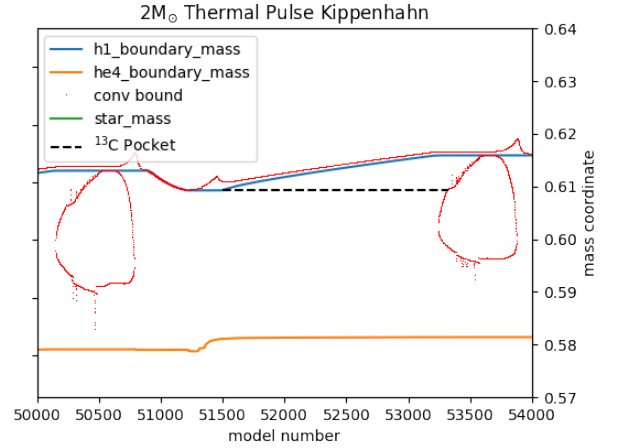


Figure 2. Within the He intershell region, the ^{13}C pocket forms and isotopic ratios are set by the s-process (Fig. 6). It is then mixed and diluted in the He-flash pulse driven convection zone where temperatures get high enough to activate $^{22}\text{Ne}(\alpha, n)^{25}\text{Mg}$. This shifts the isotopic ratios to those shown in Figure 8

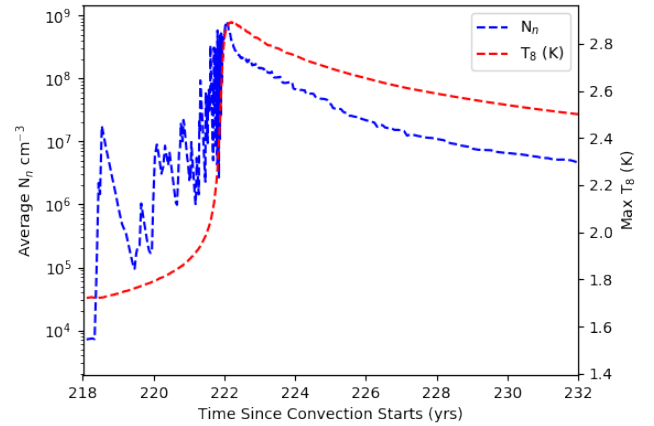


Figure 3. This is a plot of the average neutron density and maximum temperature within the convection zone as a function of time. The temperature rises very rapidly and then slowly drops. This affects the average neutron density due to the sensitivity of the $^{22}\text{Ne}(\alpha, n)^{25}\text{Mg}$ reaction to temperature and can be seen clearly in this plot.

few years. However, this will have an impact on the isotopic ratios of Zr as discussed in §2.4.

2.3 Diffusion Coefficient Modifications

The MESA models use the MLT and the diffusion equation to estimate how the mass fraction of isotopic species are transported and mixed throughout a convection zone. To calculate the change in mass fraction of a particular species at a particular mass coordinate in time, the stellar evolution

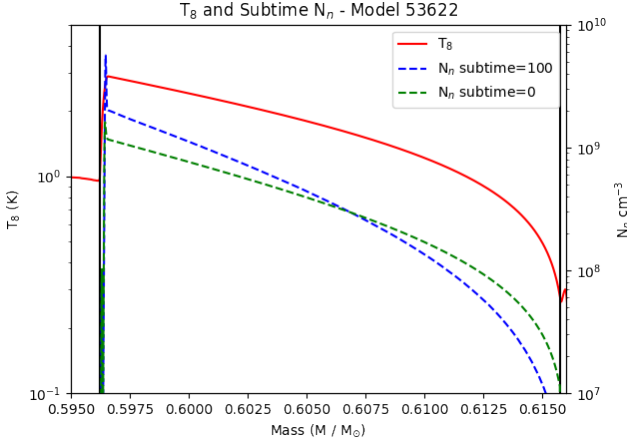


Figure 4. These are profiles from the modified diffusion data (§2.3). The black vertical lines are where the convective boundaries are located. The temperature peaks very close to the lower convective boundary and the neutron density also peaks right at that point. There is a significant change in the neutron density when sub-time steps are used. This is attempting to resolve the $^{22}\text{Ne}(\alpha, n)^{25}\text{Mg}$ reaction at the lower convective boundary.

codes solve the differential equation

$$\frac{d\mathbf{X}_i}{dt} = \frac{d\mathbf{X}_i}{dt}\bigg|_{\text{burn}} + \frac{d\mathbf{X}_i}{dt}\bigg|_{\text{mix}} \quad (2)$$

which contains the changes due to the possible reactions that the particular species can be involved in and the spatial diffusion of matter from the mixing in a convection zone. Using the diffusion formalism, this mixing term is given by

$$\frac{d\mathbf{X}_i}{dt}\bigg|_{\text{mix}} = \frac{\partial}{\partial m}[(4\pi r^2 \rho)^2 D(m) \frac{d\mathbf{X}_i}{dm}] \quad (3)$$

Where $D(m)$ is the diffusion coefficient at mass coordinate m .

Using the MLT, the diffusion coefficient is given by

$$D = \frac{1}{3} v_{\text{MLT}} \alpha_{\text{MLT}} H_p \quad (4)$$

Where $\alpha_{\text{MLT}} H_p$ is called the mixing length. By using the formalism of MLT, this diffusion would immediately go to zero at the Schwarzschild boundary (convective boundary) but overshoot is implemented and the diffusion coefficient is extended outside of the convective boundaries with use of Equation (1). The Schwarzschild boundary is the mass coordinate where the Schwarzschild criterion, the condition in which the gas will be convectively unstable, is located. The Schwarzschild criterion is when the condition

$$\nabla_{\text{rad}} > \nabla_{\text{ad}} \quad (5)$$

is satisfied. $\nabla_{\text{rad}} = \left(\frac{\partial \ln T}{\partial \ln P}\right)_{\text{rad}}$ is the gradient that the star would have if all of the energy is transported by radiation while $\nabla_{\text{ad}} = \left(\frac{\partial \ln T}{\partial \ln P}\right)_{\text{ad}}$ is the gradient the star would have if all of the energy was being transported by convection.

The functionality of the MLT diffusion coefficient across the convection zone is similar to what is calculated from 3D hydrodynamic simulations. However, a main qualitative difference is that the diffusion coefficient begins to drop well

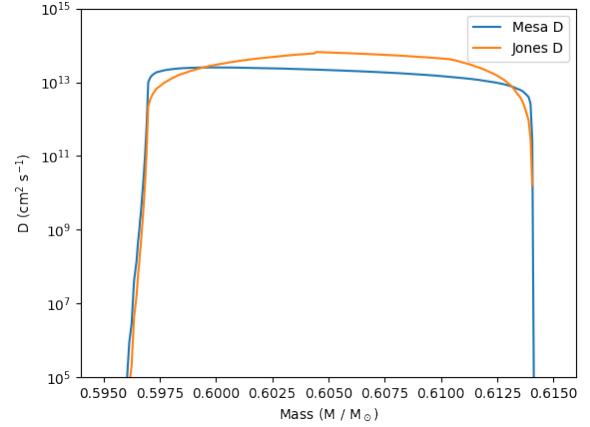


Figure 5. The MLT diffusion coefficient has a more flat profile between the convective boundaries while the diffusion coefficient given by (Jones et al. 2017) (Eq. (6)) is about an order of magnitude smaller at the convective boundaries.

before the convective boundary while the MLT diffusion coefficient will not. The reason behind this is that because the convective boundary is very stiff, an incompressible fluid would not be able to have a velocity profile that was nearly constant up to the boundary. It would need to slow down significantly as it got closer to that boundary as the fluid needs to disperse when it hits the wall with the condition that it cannot be compressed. A model for the diffusion coefficient that has been able to reproduce results from 3D hydro simulations is provided by (Jones et al. 2017). The formula for the diffusion coefficient is

$$D_{\text{hydro}} = v_{\text{MLT}} \min(\alpha_{\text{MLT}} H_p, |r - r_0|) \quad (6)$$

where $r_0 = r_{\text{SC}} - f_{\text{CBM}} H_p^{\text{SC}}$ which are quantities that are evaluated at the Schwarzschild boundary. This does not make major changes to the functionality and magnitude of the diffusion coefficient except that it falls off quicker when approaching the convective boundaries. This can be seen in Figure 5. With the temperature being highest at the lower convective boundary (Fig. 4) and with using Equation (6) for the diffusion coefficient rather than Equation (4), there would be less matter diffusing to the higher temperatures at the lower boundary. The possible nucleosynthetic consequences of this are discussed in §2.4 and shown in §3.1.

2.4 ^{95}Zr and ^{128}I Branching

Within the ^{13}C pocket, the reaction that causes the high neutron densities for the s -process is $^{13}\text{C}(\alpha, n)^{16}\text{O}$. The neutron densities do not reach $N_n \approx 5 \times 10^8 \text{ cm}^{-3}$ that are required to open the ^{95}Zr branch (Battino et al. 2016). This causes a situation in which there is production of ^{94}Zr from the s -process but due to low neutron densities not as much ^{96}Zr is produced. This can be seen from the isotope mass fractions of Zr in Fig. 6. The s -process path and ^{95}Zr branch can be seen in Figure 7

During the He-flash PDCZ temperatures get high enough for the $^{22}\text{Ne}(\alpha, n)^{25}\text{Mg}$ reaction to occur. Neutron densities can exceed the lower limit for the ^{95}Zr branching

(Fig. 3). This will shift the isotopic mass fractions of ^{96}Zr and ^{94}Zr to what is shown in Figure 8. Their mass fractions dropped significantly due to the dilution of the ^{13}C pocket into the PDCZ however the change in the ratio, $\log_{10}(^{96}\text{Zr}/^{94}\text{Zr})$, went from -2.7 to -0.9. This is caused by the opening of the ^{95}Zr branch allowing for production of ^{96}Zr . This branch is only open for a very short amount of time as the neutron density is only larger than $5 \times 10^8 \text{cm}^{-3}$ for a few years (Fig. 3) but its effects on the Zr isotopic ratios are significant.

To compare with the measurements made by Barzyk et al. (2006), the isotopic ratios need to be represented into the per mil, δ , form. For a given isotopic ratio, this is defined as

$$\delta(^{96}\text{Zr}/^{94}\text{Zr}) = \left[\left(\frac{^{96}\text{Zr}}{^{94}\text{Zr}} / \frac{^{96}\text{Zr}_{\odot}}{^{94}\text{Zr}_{\odot}} \right) - 1 \right] \times 1000 \quad (7)$$

The comparison of $\delta(^{96}\text{Zr}/^{94}\text{Zr})$ from the pre-solar grains measured by (Barzyk et al. 2006) and what stellar evolution models predict from (Battino et al. 2016) is in Figure 1.

The ^{128}I isotope is unstable with a lifetime of only 25 minutes and it has two competing branches. These reactions are the β^- decay, $^{128}\text{I}(\beta^-)^{128}\text{Xe}$, and the electron capture $^{128}\text{I}(\beta^+)^{128}\text{Te}$. The electron capture rate is very sensitive to the temperature as well as the electron density (Reifarth et al. 2004). Figure 9 shows all of the isotopes that play a role in the ^{128}I branching. Within the He-flash PDCZ the temperature peaks very close to the lower convective boundary. With the convective time scale (§2.5) during the PDCZ being only a few hours, fresh ^{127}I from the top of the convection zone will come to the bottom and can capture a neutron easily due to the very high neutron densities there. Because of the short half-life of ^{128}I , a significant portion of these will decay while being at the higher temperatures near the lower convective boundary. This will lead to a significant portion of the ^{128}I to undergo $^{128}\text{I}(\beta^+)^{128}\text{Te}$ rather than $^{128}\text{I}(\beta^-)^{128}\text{Xe}$. Since the p -process is not occurring within the He-flash PDCZ, the only production of ^{128}Xe comes from the $^{128}\text{I}(\beta^-)^{128}\text{Xe}$ and there are losses of it from neutron captures. Because of this, the $^{128}\text{Xe}/^{130}\text{Xe}$ ratio can be used as a tracer of what the dominating branch of ^{128}I is.

2.5 mppnp Post Processing

The nucleosynthesis that was calculated with the **mppnp** code used a network of over 1000 isotopes and was limited by species that have a β decay less than half a minute. Since only the s -process can happen throughout this stars evolution up to the AGB, the neutron densities will not be high enough to have significant production of species with very short β decay half lives.

From using the Ritter et al. (2017) models, the nucleosynthesis was already calculated for the $2M_{\odot}$, $Z = 0.02$, throughout its entire evolution with the MLT diffusion coefficient. To calculate models with the diffusion coefficient from Equation (6), the H5 files that the MESA data was outputted to was modified. This was simply done with python and the **mppnp** code could be run normally but it would have the modified diffusion coefficient.

Having a smaller diffusion coefficient at the lower convective boundary is expected to limit the amount of ^{22}Ne coming from the top of the convection to replenish what

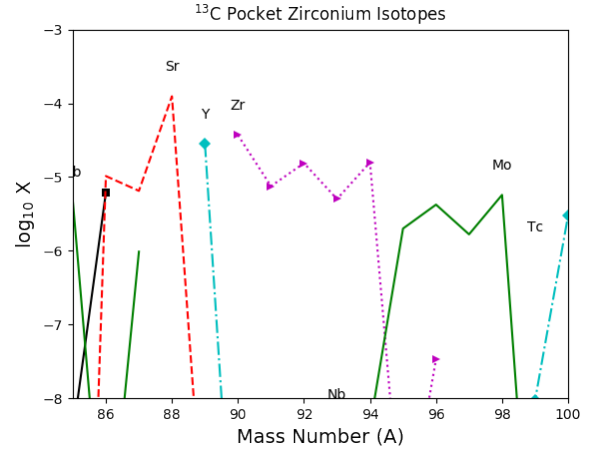


Figure 6. These isotope ratios are averaged across the ^{13}C pocket. Within the ^{13}C pocket there is a significant amount of ^{94}Zr produced but almost no ^{95}Zr . This is due to the low neutron densities not opening the ^{95}Zr branch. The logarithm base 10 of the $^{96}\text{Zr}/^{94}\text{Zr}$ ratio just before the ^{13}C pocket is absorbed into the PDCZ is approximately -2.7.

Mo 92 14.77 $\alpha = 2E-7 \pm 0.06$	Mo 93 4.9 m 3.5-10 ⁸ s $\alpha = 0.02$	Mo 94 9.23 $\alpha = 13.4$ $\alpha = 0.000030$	Mo 95 15.90 $\alpha = 0.5$	Mo 96 16.68 $\alpha = 2.5$ $\alpha = 4E-7$	Mo 97 9.56 $\alpha = 0.14$	Mo 98 24.19 $\beta^- 1.2$ $\gamma 740, 182$ $\gamma 778$ $\alpha = 2$	Mo 99 66.0 h $\beta^- 1.2$ $\gamma 740, 182$ $\gamma 778$ $\alpha = 2$
Nb 91 86.9 d $\alpha = 100$	Nb 92 10.15 d 3.8-10 ⁸ s $\alpha = 0.02$	Nb 93 15.12 s 100 $\alpha = 0.02$	Nb 94 6.26 m 2-10 ⁸ s $\alpha = 0.5$	Nb 95 86.6 h 34.97 d $\beta^- 0.7$ $\gamma 778, 569$ $\gamma 786$ $\alpha = 7$	Nb 96 23.4 h $\beta^- 0.7$ $\gamma 778, 569$ $\gamma 786$ $\alpha = 7$	Nb 97 53 s 74 m $\beta^- 1.3$ $\gamma 740, 182$ $\gamma 778$ $\alpha = 2$	Nb 98 81 m 2.9 s $\beta^- 1.3$ $\gamma 740, 182$ $\gamma 778$ $\alpha = 2$
Zr 90 51.45 $\alpha = 0.014$	Zr 91 11.22 $\alpha = 1.2$	Zr 92 17.15 $\alpha = 0.2$	Zr 93 1.5-10 ⁸ a $\alpha = 0.06$ $\alpha = 4$	Zr 94 17.38 $\alpha = 0.049$	Zr 95 64.0 d $\beta^- 0.4$ $\gamma 757, 724$ $\gamma 786$ $\alpha = 7$	Zr 96 2.80 $\beta^- 1.9$ $\gamma 508, 1148$ $\gamma 555$ $\alpha = 2$	Zr 97 16.8 h $\beta^- 1.9$ $\gamma 508, 1148$ $\gamma 555$ $\alpha = 2$
Y 89 16.8 s 100 $\alpha = 100$	Y 90 3.19 h 64.1 h 49.7 m 58.5 d $\beta^- 1.8$ $\gamma 934, 1405$ $\gamma 951, 448$ $\alpha = 1$	Y 91 49.7 m 58.5 d $\beta^- 1.8$ $\gamma 934, 1405$ $\gamma 951, 448$ $\alpha = 1$	Y 92 3.54 h $\beta^- 2.9$ $\gamma 267, 947$ $\gamma 1918$ $\alpha = 7$	Y 93 10.1 h $\beta^- 4.9$ $\gamma 919, 1139$ $\gamma 551$ $\alpha = 7$	Y 94 18.7 m $\beta^- 4.4$ $\gamma 954, 2176$ $\gamma 3577, 1324$ $\gamma 2932$ $\alpha = 2$	Y 95 10.3 m $\beta^- 1.9$ $\gamma 508, 1148$ $\gamma 555$ $\alpha = 2$	Y 96 8.6 s 5.34 s $\beta^- 1.9$ $\gamma 508, 1148$ $\gamma 555$ $\alpha = 2$
Sr 88 82.58 $\beta^- 1.5$	Sr 89 50.5 d $\beta^- 0.8$	Sr 90 28.64 a $\beta^- 1.1$ $\gamma 27$	Sr 91 9.5 h $\beta^- 1.1$ $\gamma 27$	Sr 92 2.71 h $\beta^- 1.1$ $\gamma 27$	Sr 93 7.45 m $\beta^- 1.1$ $\gamma 27$	Sr 94 74 s $\beta^- 1.1$ $\gamma 27$	Sr 95 24.4 s $\beta^- 1.1$ $\gamma 27$

Figure 7. In order for there to be significant production of ^{96}Zr the neutron densities must be high enough such that the ^{95}Zr (half-life 64 days) does not all decay to ^{95}Nb . The ^{95}Zr formed from the $^{94}\text{Zr}(n, \gamma)^{95}\text{Zr}$ reaction.

was lost from the $^{22}\text{Ne}(\alpha, n)^{25}\text{Mg}$ reaction. However, if a time step is so large that many convective turnover times have passed, this effect will not be observed. By default, **mppnp** will take a time step that the stellar evolution model (MESA) took but evenly spaced sub-time steps between these can be taken. This is of course due to the fact that **mppnp** needs to utilize the thermodynamic quantities of the star at a particular point in time to compute the nucleosynthesis. In order to estimate how many sub-time steps are needed to resolve the convection, the convective time scale was calculated. With using MLT, the parcels of matter that convect have a velocity, v_{MLT} , and travel a mixing length on average. So the convective time scale is approximately

$$\tau_{\text{conv.}} \approx \frac{\alpha_{\text{MLT}}}{v_{\text{MLT}}} \quad (8)$$

The convective time scale was calculated at every model number that had the He-flash PDCZ and was plotted with

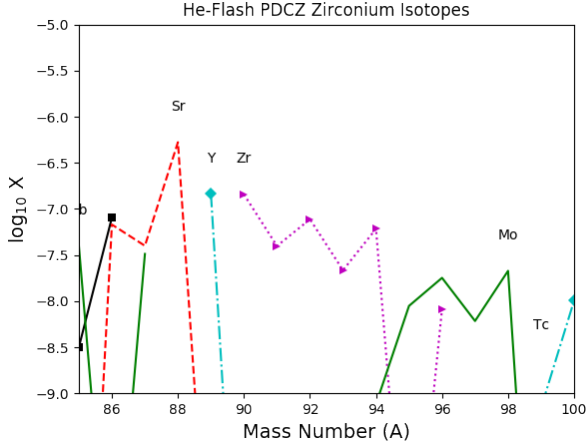


Figure 8. These isotope ratios are averaged across the He-flash PDCZ. After the ^{13}C pocket is mixed into the He-flash PDCZ, the temperatures get high enough for the $^{22}\text{Ne}(\alpha, n)^{25}\text{Mg}$ reaction. This provides high enough neutron densities to open the ^{95}Zr branch and boost the ^{96}Zr . The logarithm base 10 of the $^{96}\text{Zr} / ^{94}\text{Zr}$ ratio after the PDCZ is approximately -0.9.

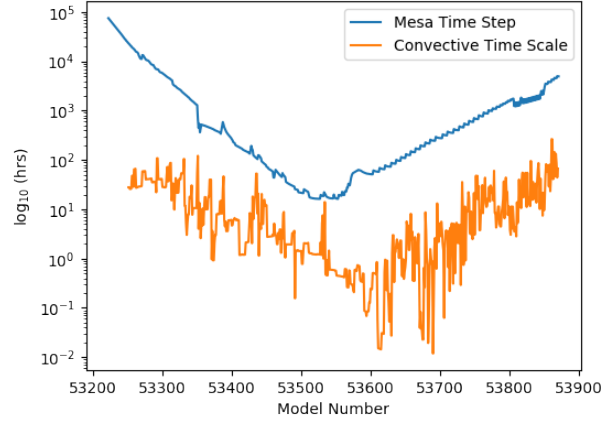


Figure 10. The time steps used by MESA are generally 100 times longer than the convective time scale at that model number. In order to resolve the impact of the hydro diffusion coefficient on the Zr isotopic ratios, the convection needs to be resolved. A sub-time step of 100 for `mppnp` allows for this.

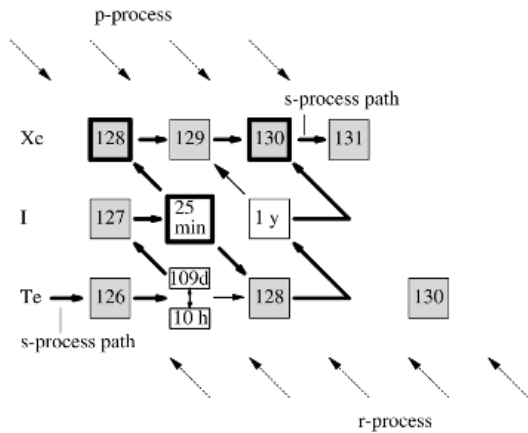


Figure 9. The unstable isotope, ^{128}I , can either β^- decay or capture an electron (β^+). The electron capture branching is very sensitive to the temperature. If it β^- decays there will be production of ^{128}Xe . If it captures an electron, it will decay to ^{128}Te leading to no production of ^{128}Xe . Losses of ^{128}Xe are from neutron captures. This figure is from (Reifarth et al. 2004).

the time step that the MESA model took at that point. This is shown in Figure 10. From this, if 100 sub-time steps are taken the convection can be resolved. The number of sub-time steps that were taken when `mppnp` was used with the $2M_{\odot}$, $Z = 0.02$, MESA model was 100.

Another thing to consider is the notion that the only way to know if a numerical result is something that is realistic with the models that were used to compute it, there needs to be numerical convergence. To achieve this, the resolution, or in this case number of time steps, needs to be increased to see if there are changes with the numerical results. If there are very minor changes, the solution that is

found can be considered converged. In Figure 4, the neutron density is measured with two different time steps and are plotted as a function of mass. The neutron density determined with 100 sub-time steps is about six times as large at the mass coordinate of maximum temperature. This shows that the neutron densities were not converged with the zero sub-time steps for the modified diffusion coefficient models. If more time was spent on this work, a few more sub-time steps would have been chosen to check if this 100 sub-time solution is in fact converged.

3 RESULTS

3.1 Effects on $\delta(^{96}\text{Zr} / ^{94}\text{Zr})$

After running `mppnp` on the MESA H5 files with modified diffusion coefficients and 100 sub-time steps, the $\delta(^{96}\text{Zr} / ^{94}\text{Zr})$ was calculated throughout the thermal pulse. This is shown in Figure 11. Only the last 300 models were calculated due to the computational time needed. They were chosen such that the models with the highest temperatures, where the highest neutron densities would be, were computed. The values of $\delta(^{96}\text{Zr} / ^{94}\text{Zr})$ that matter are after the He-flash PDCZ has finished. These are the isotopic ratios that will be drawn to the surface by the third dredge up. In Figure 11, the $\delta(^{96}\text{Zr} / ^{94}\text{Zr})$ is an average value across the maximum extent of the PDCZ for each model number. The $\delta(^{96}\text{Zr} / ^{94}\text{Zr})$ from the zero sub-time steps modified diffusion model produced results that were not expected. The $\delta(^{96}\text{Zr} / ^{94}\text{Zr})$ increased meaning that the $^{96}\text{Zr} / ^{94}\text{Zr}$ ratio increased while it was expected to decrease due to the supposed smaller neutron densities as discussed in §2.2. However, it is likely that this model is not realistic as it may not have been converged as the 100 sub-time step model provided entirely different results. In fact, these results are what had been expected as the number density of ^{96}Zr has decreased from the decrease in neutron density.

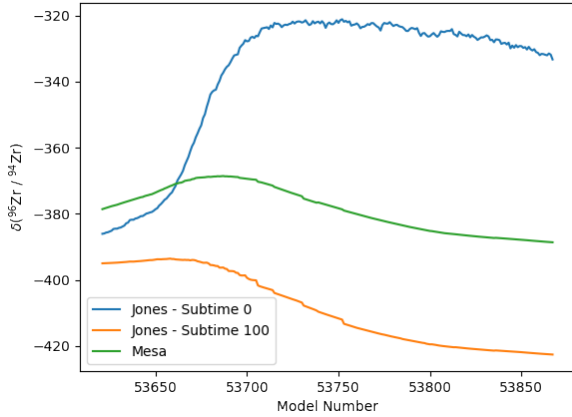


Figure 11. At the end of the convection zone (the last model number), the $\delta(^{96}\text{Zr}/^{94}\text{Zr})$ from the 100 sub-time step model with the modified diffusion coefficient is significantly lower than the same quantity from the original nucleosynthesis results. The no sub-time step model shows very unintuitive results.

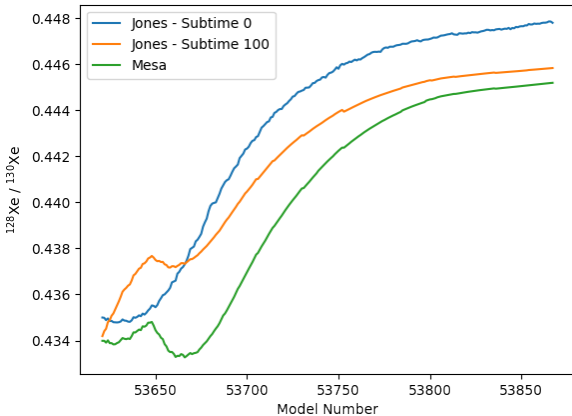


Figure 12. At the end of the convection zone (the last model number), the $^{128}\text{Xe} / ^{130}\text{Xe}$ ratio does not change much. It appears as though the ^{128}I branch is not affected by the changes to the diffusion coefficient.

3.2 The $^{128}\text{Xe} / ^{130}\text{Xe}$ Ratio

With the same data as what was used in the previous section, a similar analysis was conducted for the $^{128}\text{Xe} / ^{130}\text{Xe}$ ratio. They were averaged results across the maximum extent across the PDCZ and they are shown in Figure 12. At the end of the PDCZ, the $^{128}\text{Xe} / ^{130}\text{Xe}$ ratio for the 100 sub-time step model did not change significantly from the baseline models. The expectation was that the $^{128}\text{I}(\beta^+)^{128}\text{Te}$ reaction would occur less frequently as there would be less of it at the highest temperatures in the PDCZ. One possibility for the insignificant change is that this reaction had not been resolved with the time steps chosen. The half-life of ^{128}I is only 25 minutes while the time steps that were used were not smaller than a few hours (Fig. 10).

4 CONCLUSIONS

The $2M_{\odot}, Z = 0.02$, stellar model from Ritter et al. (2017) was modified by changing the diffusion coefficients to the model stated in Jones et al. (2017), Equation (6). The post-processing nucleosynthesis was computed with `mppnp` and 100 sub-time steps were used to resolve the convection. The $\delta(^{96}\text{Zr} / ^{94}\text{Zr})$ and $^{128}\text{Xe} / ^{130}\text{Xe}$ were averaged across the maximum extent of the PDCZ. These are the isotopic ratios that would be mixed into the H envelope from the third dredge up and can be measured in the SiC grains that would form when this mass is lost from stellar winds during the AGB phase.

The $^{128}\text{Xe} / ^{130}\text{Xe}$ ratio that was measured with the modified diffusion coefficients and 100 sub-time steps was not significantly different from the baseline MESA model, `mppnp` post processed predictions. This may be due to not resolving the ^{128}I branching as the sub-time steps amounted to a few hours while its half-life is only 25 minutes.

The $\delta(^{96}\text{Zr} / ^{94}\text{Zr})$ measured cannot directly be compared with results from (Battino et al. 2016) as theirs are measured after being mixed into the H envelope. There is also the fact that the results from this work are only due to one PDCZ, the 24th, and the feedback effects from this happening many times is not taken into account. However, the results do state that the $\delta(^{96}\text{Zr} / ^{94}\text{Zr})$ from the modified diffusion coefficient is less than the other models which would better match the observations found in (Barzyk et al. 2006). To fully quantify the effects the modified diffusion coefficient would have on the Zr isotopic ratios, this would need to be applied to all thermal pulses throughout the AGB phase. These results are based on the assumption that this solution has converged but no test has definitively shown this.

ACKNOWLEDGEMENTS

I would like to acknowledge the suggestions and input that Falk Herwig had throughout my undertaking of this project. His guidance allowed for the completion of this project in the limited time frame that I had.

REFERENCES

- Barzyk J. G., Savina M. R., Davis A. M., Gallino R., Pellin M. J., Lewis R. S., Amari S., Clayton R. N., 2006, *New Astron. Rev.*, **50**, 587
- Battino U., et al., 2016, *ApJ*, **827**, 30
- Cox J. P., Giuli R. T., 1968, Principles of stellar structure
- Freytag B., Ludwig H.-G., Steffen M., 1996, *A&A*, **313**, 497
- Herwig F., 2000, *A&A*, **360**, 952
- Jones S., Andrassey R., Sandalski S., Davis A., Woodward P., Herwig F., 2017, *MNRAS*, **465**, 2991
- Paxton B., Bildsten L., Dotter A., Herwig F., Lesaffre P., Timmes F., 2011, *ApJS*, **192**, 3
- Reifarth R., Käppeler F., Voss F., Wisshak K., Gallino R., Pignatari M., Straniero O., 2004, *ApJ*, **614**, 363
- Ritter C., Herwig F., Jones S., Pignatari M., Fryer C., Hirschi R., 2017, preprint, ([arXiv:1709.08677](https://arxiv.org/abs/1709.08677))

This paper has been typeset from a \LaTeX file prepared by the author.